AGU PUBLICATIONS

Geochemistry, Geophysics, Geosystems

Supporting Information for

Slow Geodynamics and Fast Morphotectonic in the far East Tethys

L. Husson[1]†, N. Riel[2], S. Aribowo[1,3], C. Authemayou[4], G. de Gelder[1], B. J.P. Kaus[2], C. Mallard[5], D. H. Natawidjaja[3], K. Pedoja[6], A. C. Sarr[7]

[1] Institut des Sciences de la Terre, Université Grenoble Alpes, Grenoble, France.

[2] Institute of Geosciences, Johannes Gutenberg University Mainz, J.-J.-Becher-Weg 21, D-55128, Mainz, Germany.

[3] Research Center for Geotechnology, Indonesian Institute of Sciences (LIPI), Bandung, Indonesia.

[4] LGO, IUEM, CNRS, Université de Brest, Plouzané, France.

[5] School of Geosciences, University of Sydney, Sydney, Australia.

[6] M2C, Université de Caen, France.

[7] CEREGE, Aix-Marseille Université, France.

† Corresponding author: Laurent Husson (laurent.husson@univ-grenoble-alpes.fr)

Contents of this file

Text S1
Figures S1 to S10
Table S1

Additional Supporting Information (Files uploaded separately)

Captions for Movies S1 to S2

Introduction

The following material gives technical details on the modeling technique and modeling approach used to develop the study, as well as the compilation of data from the literature and complementary data.

Text S1: Modeling strategy and additional simulations:

The initial surface layout of the lithosphere of the 5 different setups explored in this study are presented as top views in Figure S3. Setups I and II represent simplified frameworks of the SE Asia system ~25 Myr ago. In these setups, the Australian plate is simplified as an 1800 km wide square plate. In model I Sundaland is simplified as a square shape of similar size while in model II the front edge of Sundaland is curved to account for the actual curvature of the Java-Sumatra trench. Models III, IV and V are variations of a more realistic plate configurations mostly adapted from the reconstructions *(5,8,10,11,16)*. The simulation integrates the Sula Spur, a land promontory that belongs to the Australian continent and circumscribes the Banda embayment on its northern side. Model III shows a simplified trench line, nearly straight from the eastern to the western wall of the model, while model IV uses a more complex trench line. In both models III and IV, Wallacea is solely made up of an oceanic lithosphere. Model V (preferred simulation, see main text) geodynamic reconstruction. In this setup, Wallacea exhibits a more complex tessellation of oceanic and continents lithosphere (including Sulawesi continental block, and an agglomerated package of islands that represents the archipelago of very small unit prior to the collision, now distributed from Halmahera to the Bird's Head and Western Papua). In all simulations, the Indian plate is initially subducting below a thinner and narrow (< 300km) overriding continental plate margin representing the volcanic arc.

Model I (Fig. S4)
The subduction of the Indian plate below the overriding plate (Fig. S4A) leads to collision of northern Australia at ca. 20 Myr (model time, Fig. S4B). Subsequent slab breakoff of the slab along the northern margin of Australia occurs between 20 and 30 Myr (Fig. S4B,C). After slab breakoff the system locks and no subduction polarity reversal is observed along the southern margin of the Philippine plate (Fig. S4D-F). The slowdown of convergence and absence of subduction polarity reversal can be attributed to the relatively short along trench distance between the Sundaland and Australia continental units, which leads to strong lateral coupling during collision and ultimately to results in a lockdown of the convergent system (Fig. S4D-F). Although model I captures the subsidence of Sundaland and Sahul during collision (Fig. S4B-D), the Indian plate slab breakoff along the northern, and the system lock down do not match other essential geodynamic features such as slab rollback in the Banda embayment.

Model II (Fig. S5)
Simulation II yields nearly identical results with respect to simulation I. The curvature to the Java-Sumatra trench does not influence the overall geodynamics of the system. The only noticeable difference is marked by a slightly less pronounced subsidence of Sundaland (Fig. S5B-D).

Model III (Fig. S6)
The collision initiated at the northwestern tip of the Sula spur between 4 and 17 Myr (model time, Fig. S6A,B). During that stage, the slab breaks off at the collision point and then propagates eastwards until 31 Myr (Fig. S6D). As the northern Australian promontory is being transferred along eastern Sundaland (Fig. 6B-E), subduction of Wallacea starts and slab polarity reverses along the southern margin, underneath Australia (Fig. S6D-E). Similar to simulations I and II Sundaland dynamically subsides above the subducting Indian lithosphere (Fig. S6B-D). After 36.6 Myr, the southward subduction of Wallacea takes over the global system and the Banda oceanic plate is not being subducted nor rolls back into the Banda embayment. Regardless, after the first collision of the Sula spur between 4 and 17 Myr, the model fails to reproduce first order characteristics of the convergent system.

Model IV (Fig. S7)

Initial conditions of simulation IV are comparable to those of simulation III with the exception of a less pronounced land promontory at the northern margin of Australia plate and in the initial geometry of the trench (Fig. S7A). Collision between northern Australian promontory occurs between 4.7 and 10.2 Myr (model time, Fig. S7A,B). Contrary to model III, slab breakoff occurs nearly synchronously along the margin as a consequence of its orientation with respect to the Australian margin. While subduction initiation and slab polarity reversal along the southern edge of Wallacea is observed as in simulation III, simulation IV also shows subduction initiation and rollback of the Banda oceanic slab (Fig. 7D-F). Although this simulation captures most geodynamic characteristics, it does not strictly match the timing of events, and the geometry of some tectonic features.

Model V (Fig. S8)
Simulation V is the preferred model presented in the main manuscript. Most outcomes compare to simulation IV but simulation V better adjusts with the kinematics and tectonic framework. The main differences with models III and IV are: a smaller Sula spur, and the addition of continental units in Wallacea (Fig. S8A). In this simulation, the smaller promontory allows the subduction to wrap around and to form the Banda arc, while the Sulawesi continent blocks increases the buoyancy of Wallacea, which delays subduction initiation and polarity reversal (Fig. S8D-F).

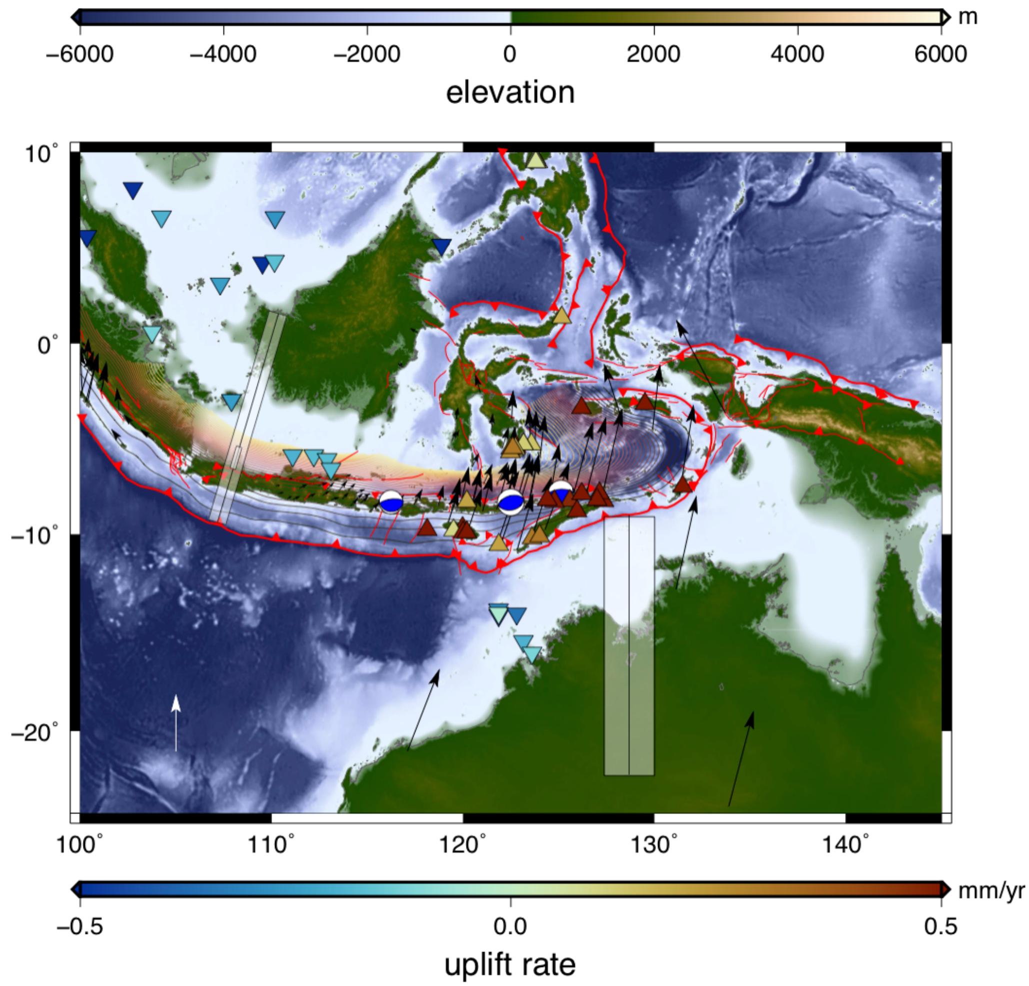

Fig. S1: Morphotectonic map of SE Asia. Tectonic structures (faults: red curve; subduction trenches: red bold curves), envelope of the subducting plate (depth isocontours 20 m), uplift rates (triangles, see Materials and Methods), selected focal mechanisms (Mw>6.5, Wetar-Flores backarc thrust), geodetic velocities *(21)*, gray bar in Sahul shows approximate location of swath profile as in Fig. 5, gray bars in Sundaland show the location of predicted profile and location of composite seismic profile (small bar) as in Fig. 7.

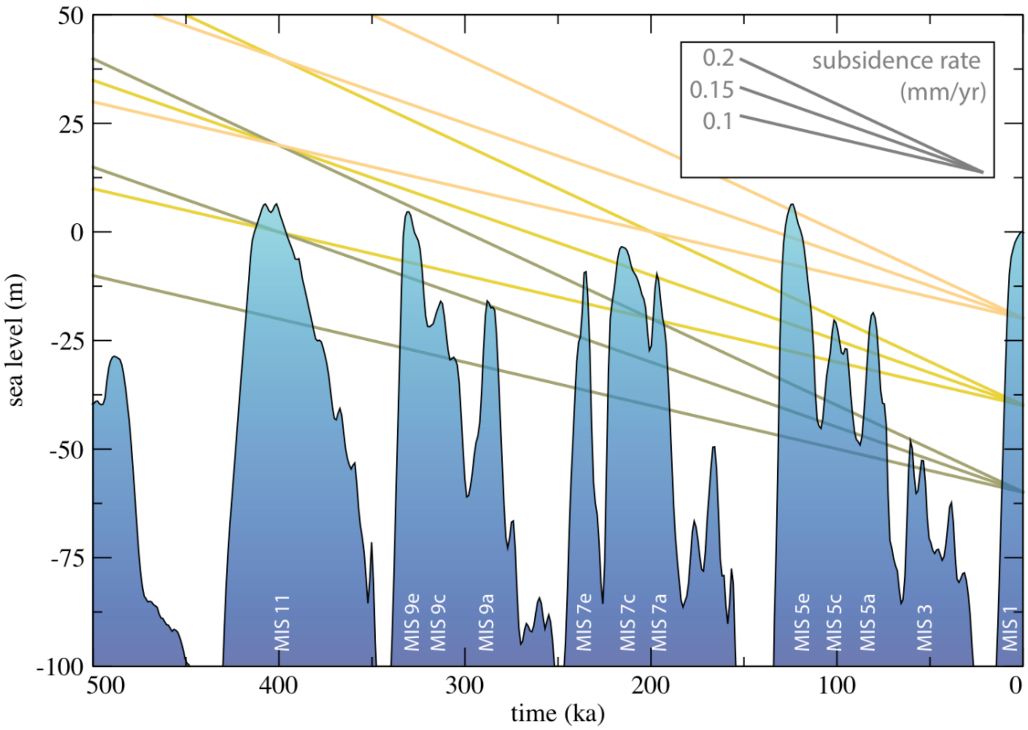

Fig. S2: Graphic derivation of subsidence rates from high resolution seismic stratigraphy. The number of incised sedimentary units is contingent on the bathymetry, sea level oscillations, and subsidence rates. Each time a subsidence line crosses the sea level curve *(53)* the stratigraphic series are fingerprinted by a river-incised sedimentary unit (corresponding to the main Marine Isotopic Stages) or sedimentary subunit (Marine Isotopic substages).

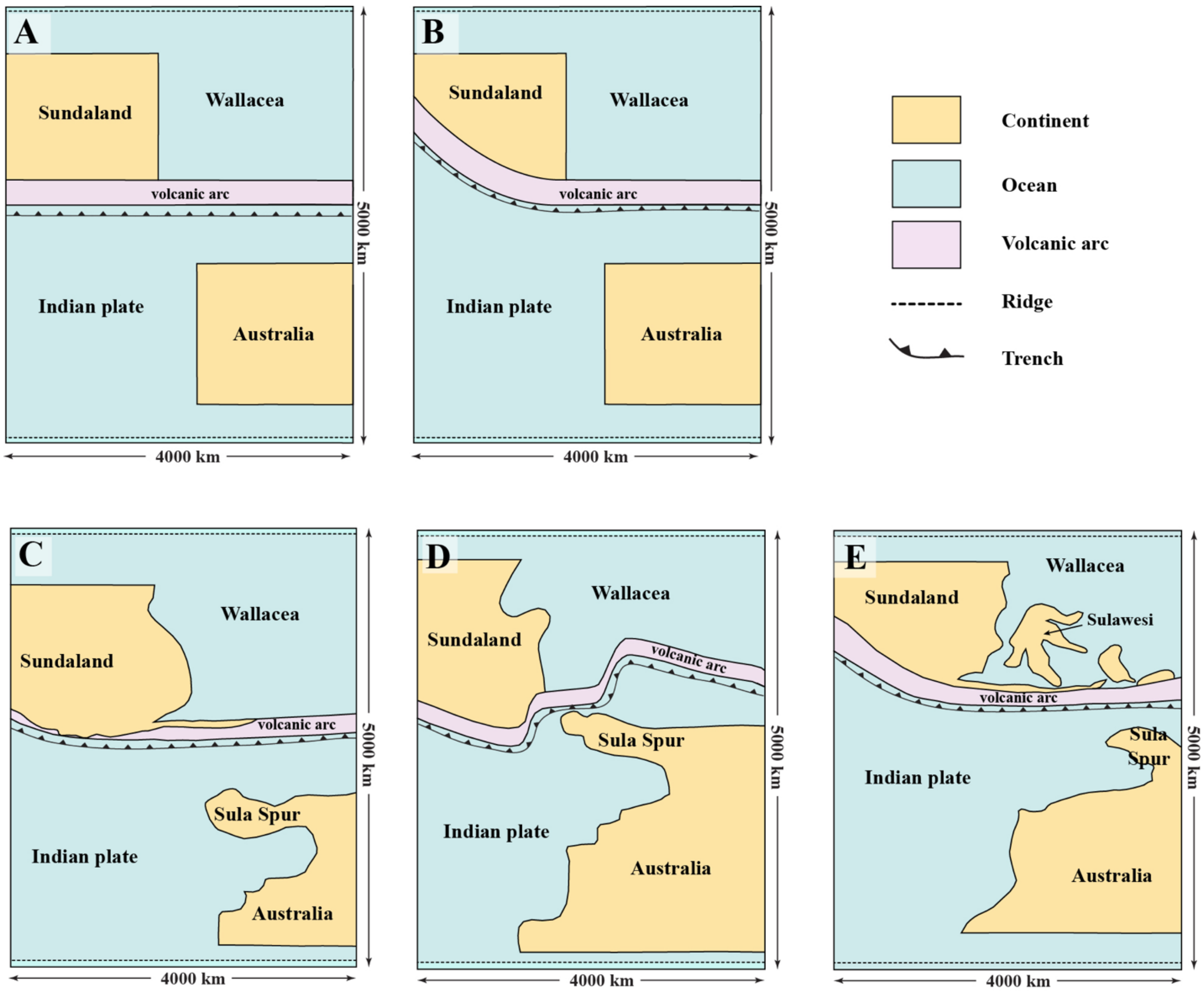

Fig. S3: Alternative model setups. Reference simulation corresponds to panel E.

Model I

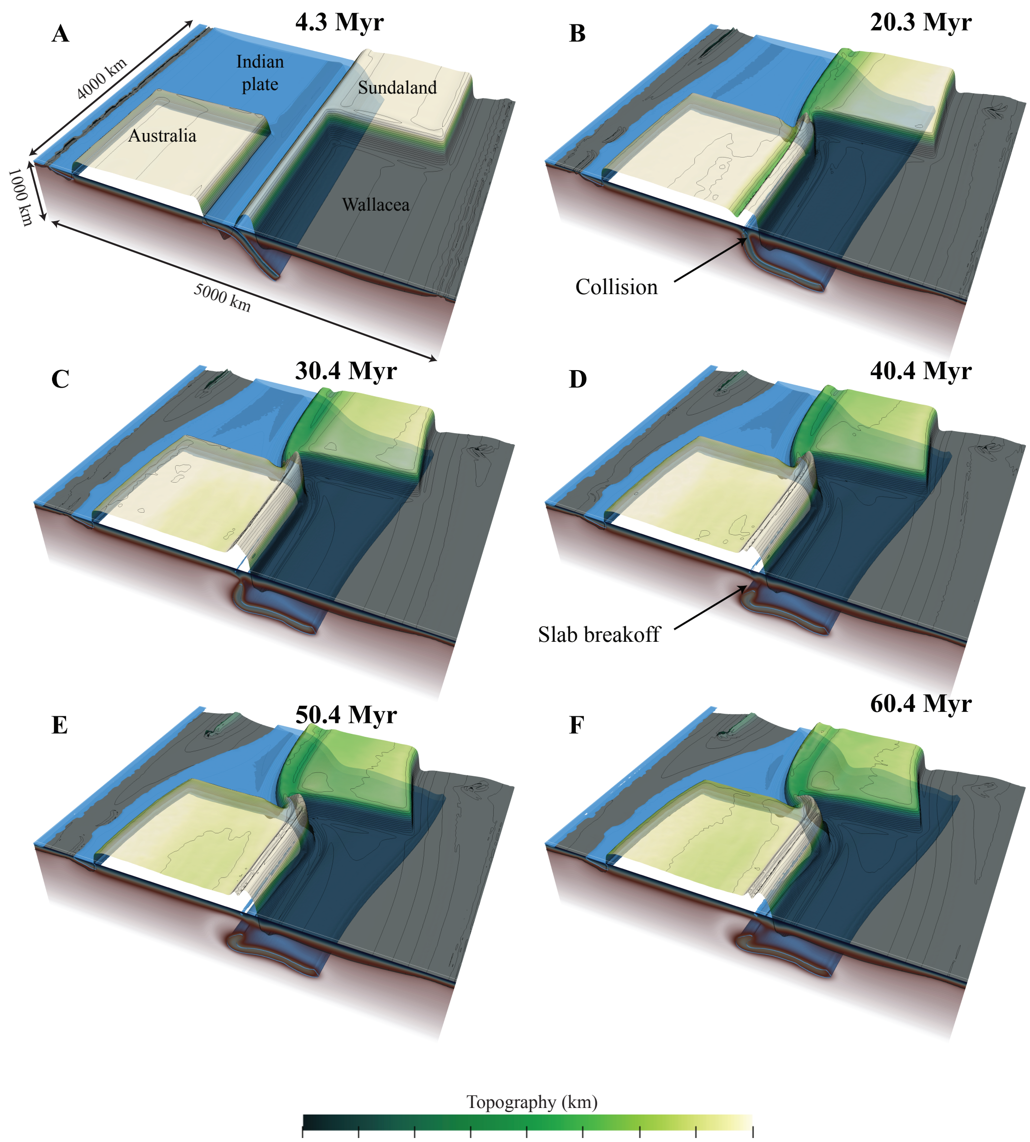

Fig. S4: simulation #1

Model II

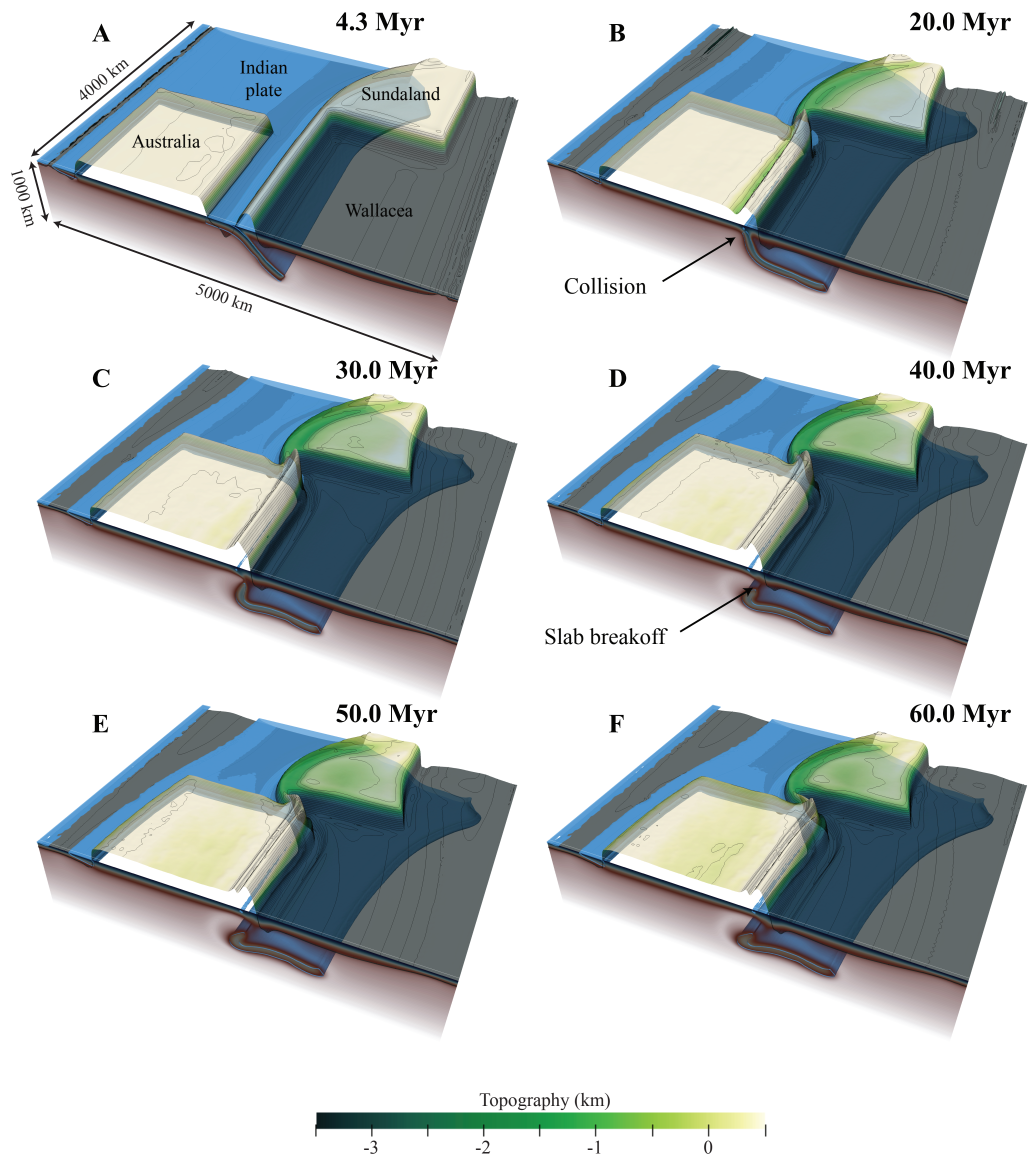

Fig. S5: simulation #2

Model III

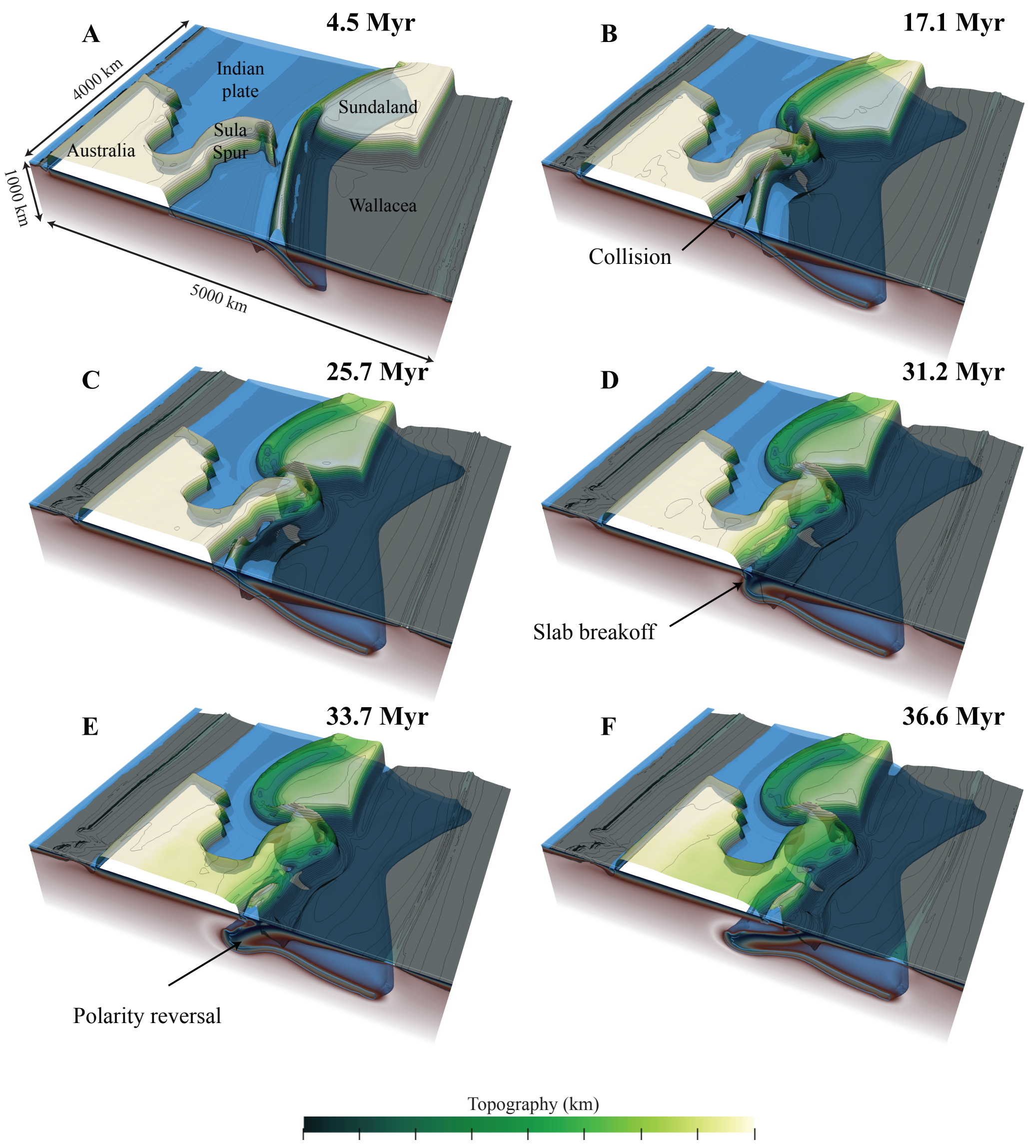

Fig. S6: simulation #3

Model IV

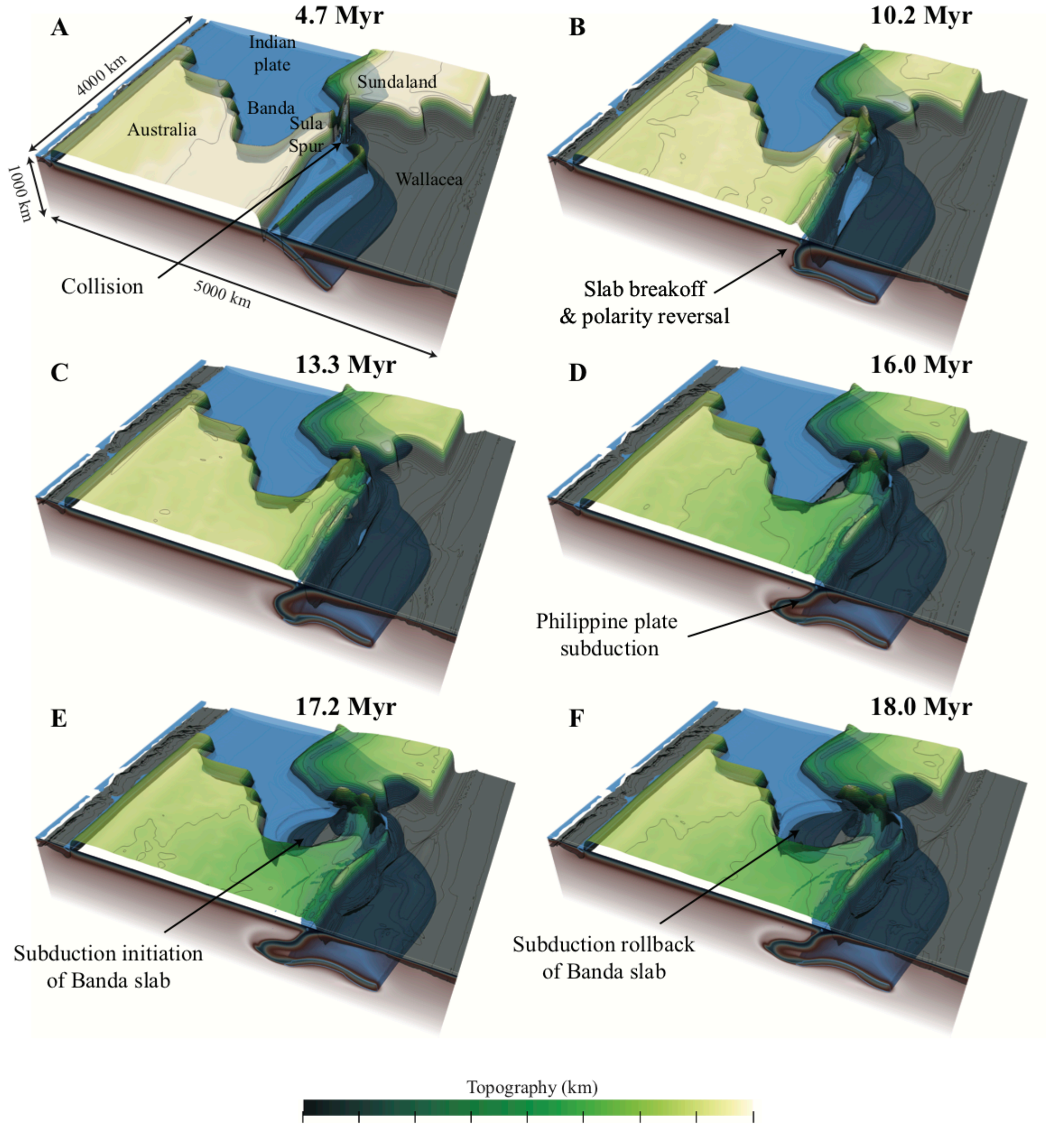

Fig. S7: simulation #4

Model V

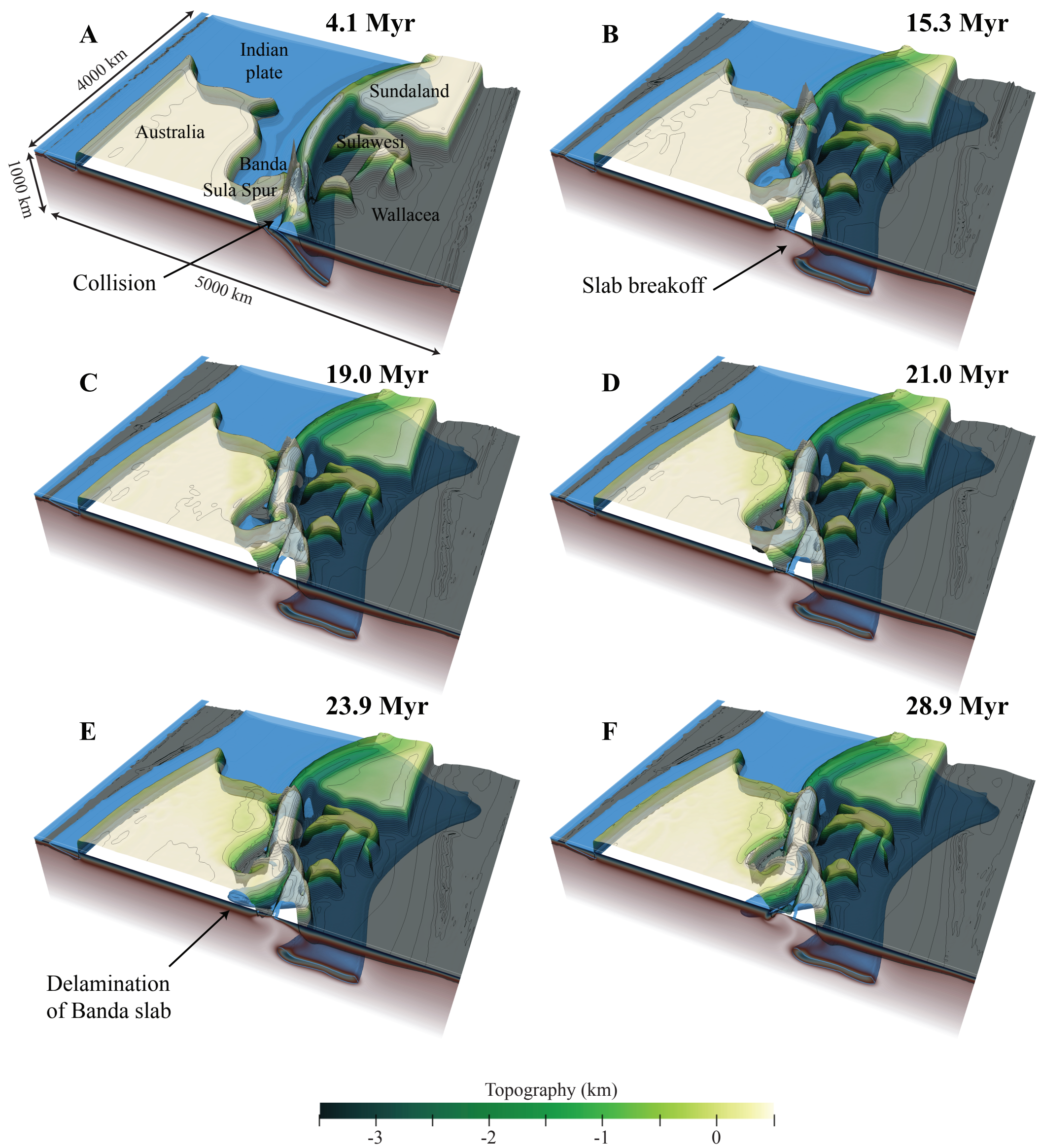

Fig. S8: simulation #5 (reference simulation)

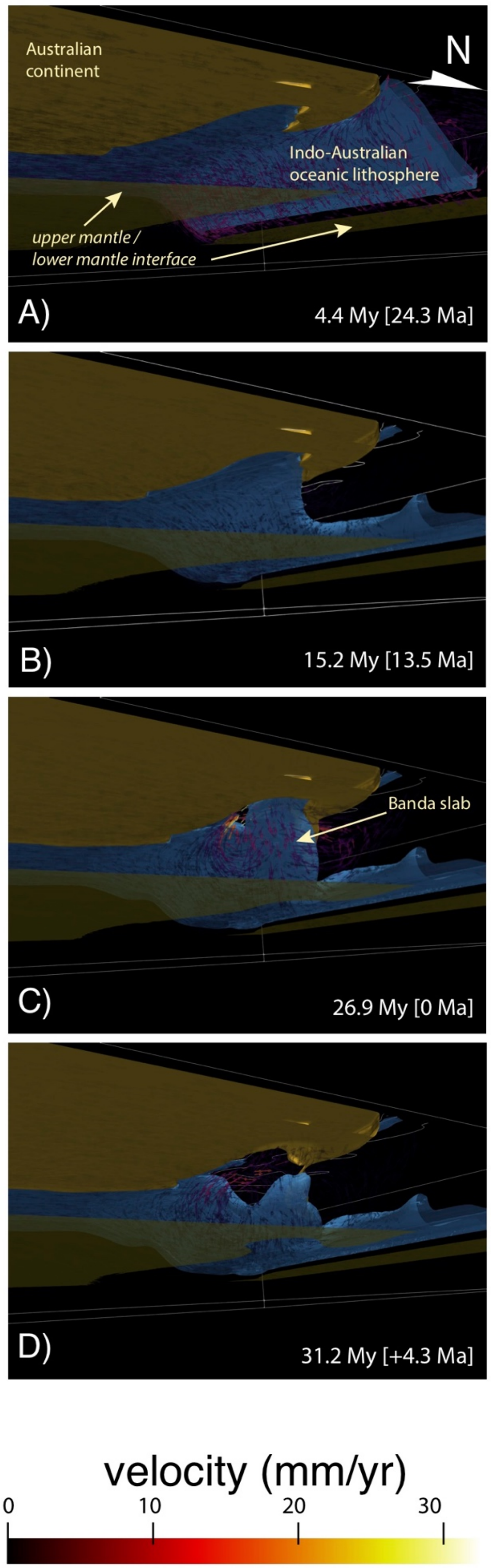

Fig. S9: Subduction dynamics, viewed from below. Vectors indicate mantle flow. The oceanic lithosphere is in blue, the Australian continent in brown, the upper/lower mantle interface in gray.

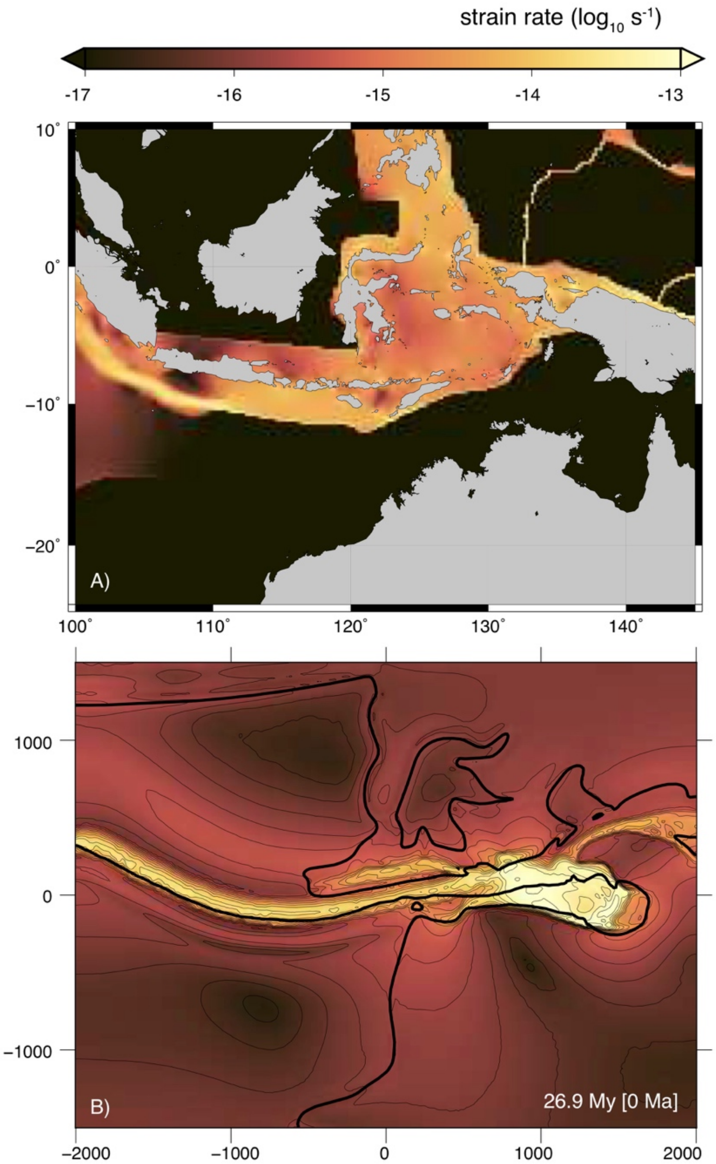

Fig. S10: observed and modeled strain rates. "Observed" strain rates are as interpolated in the World Strain Map (Kreemer et al., 2014). Both maps show focused deformation in the Banda embayment, and westward propagation of the back-arc thrust into the Sunda shelf, to the North of Java island, and equally to the north of Papua. Sulawesi is less prone to deformation in our simulation than in the World Strain Map.

latitude	longitude	Uplift rate	Reference
6.65	104.24	-0.2	Alqahtani et al. (2015)*
0.6	103.75	-0.125	Bird et al. (2006)
-8.26	125.58	0.475	Chappell and Veeh (1978)
-14.18	121.86	-0.45	Collins et al. (2011)
-13.89	121.85	-0.29	Collins et al. (2011)
-15.5	123.15	-0.2	Collins and Testa (2010)
-14.07	121.86	-0.04	Collins and Testa (2010)
-3.39	126.19	0.75	DeSmet et al. (1989)
-3.18	129.51	2.5	DeSmet et al. (1989)
-7.52	131.48	0.5	DeSmet et al. (1989)
-8.8	125.96	10.0	DeSmet et al. (1989)
-5.44	122.77	0.75	Fortuin et al. (1990)
3.14	107.31	-0.25	Hanebuth et al. (2011)
4.24	109.52	-0.95	Hanebuth et al. (2011)
-8.29	124.77	1.1	Hantoro et al. (1994)
-8.27	127.36	0.5	Harris et al. (2009)
-10.55	121.87	0.2	Harris et al. (2009)
-9.76	118.12	0.5	Harris et al. (2009)
-10.2	123.6	0.3	Jouannic et al. (1988)
-7.87	127.13	0.55	Major et al. (2013)
-9.9	120.2	0.6	Miller et al. (2021)
-10.1	124.0	0.3	Miller et al. (2021)
-8.2	127.0	0.8	Miller et al. (2021)
-8.3	120.2	0.2	Miller et al. (2021)
-8.2	124.4	1.0	Miller et al. (2021)
-7.9	126.2	0.6	Miller et al. (2021)
8.13	102.75	subsidence	Morley and Westaway (2006)
-9.8	119.5	0.1	Nexer et al. (2015)
-9.9	120.0	0.5	Nexer et al. (2015)
5.63	100.34	subsidence	Parham et al. (2016)
5.17	118.88	subsidence	Parham et al. (2016)
-5.31	123.57	0.14	Pedoja et al. (2018)
-5.31	123.16	0.12	Pedoja et al. (2018)
-5.64	122.65	0.16	Pedoja et al. (2018)
-5.31	123.16	0.12	Pedoja et al. (2018)
-5.54	122.73	0.14	Pedoja et al. (2018)
-5.53	122.5	0.29	Pedoja et al. (2018)
-5.72	122.47	0.25	Pedoja et al. (2018)
-5.5	122.6	0.3	Pedoja et al. (2018)
-9.67	119.98	0.49	Pirazzoli et al. (1993)
9.7	123.8	0.075	Ringor et al. (2004)
9.5	123.9	0.19	Ringor et al. (2004)
9.6	123.8	0.07	Ringor et al. (2004)
9.5	123.8	0.07	Ringor et al. (2004)
-2.99	107.9	-0.25	Sarr et al. (2019)*
-16.09	123.6	-0.12	Solihuddin et al. (2015)
1.36	125.16	0.18	Sumosusastro et al. (1989)
-5.9	*111.1*	*-0.2*	*Susilohadi and Soeprapto (2015)**
-5.9	*112.2*	*-0.175*	*Susilohadi and Soeprapto (2015)**
-6.1	*112.9*	*-0.175*	*Susilohadi and Soeprapto (2015)**

-6.6	*113.1*	*-0.175*	*Susilohadi and Soeprapto (2015)**
6.61	110.17	-0.27	Wong et al. (2003)
4.33	110.15	-0.17	Wong et al. (2003)

Table S1: mean Pleistocene uplift and subsidence rates, from published and new (italicized) estimates. *For subsidence rates derived from shallow seismic stratigraphy, see graphical depiction of the method on Fig. S4. References below.

Alqahtani, F.A., Johnson, H.D., Jackson, C.A.-L., Som, M.R.B. (2015). Nature, origin and evolution of a Late Pleistocene incised valley-fill, Sunda Shelf, Southeast Asia: Sedimentology, 62, 1198-1232. doi: 10.1111/sed.12185.

Bird, M. I., Pang, W. C., Lambeck, K. (2006). The age and origin of the straits of Singapore: Palaeogeography, Palaeoclimatology, Palaeoecology, v241, 531–538. doi: 10.1016/j.palaeo.2006.05.003.

Chappell J., Veeh H. (1978). Late quaternary tectonic movements and sea-level changes at Timor and Atauro island: Geological Society of America Bulletin, 89, 356–368.

Collins L. B., Testa V. (2010). Quaternary development of resilient reefs on the subsiding Kimberley continental margin, Northwest Australia: Brazilian Journal of Oceanography, 58, 67–77. doi : 10.1590/S1679-87592010000500007.

Collins L. B., Testa V., Zhao J., Qu D. (2011). Holocene Growth History and Evolution of the Scott Reef Carbonate Platform and Coral Reef: Journal of the Royal Society of Western Australia, 94, 239-250.

De Smet M., Fortuin A., Tjokrosapoetro S., Van Hinte J. (1989). Late cenozoic vertical movements of non-volcanic islands in the Banda arc area: Netherlands Journal of Sea Research, 24, 263–275. doi: 10.1016/0077-7579(89)90153-1.

Fortuin, A. R., De Smet, M. E. M., Hadiwasastra, S., Van Marle, L. J., Troelstra S. R., Tjokrosapoetro, S. (1990). Late Cenozoic sedimentary and tectonic history of south Buton, Indonesia, Journal of Southeast Asian Earth Sciences 4(2): 107-124.

Hanebuth, T. J.J, Voris, H. K., Yokoyama, Y., Saito, Y., Okuno, J. (2011). Formation and fate of sedimentary depocentres on Southeast Asia's Sunda Shelf over the past sea-level cycle and biogeographic implications: Earth-Science Reviews, 104, 92-110. Doi: 10.1016/j.earscirev.2010.09.006.

Hantoro W., Pirazzoli P. A., Jouannic C., Faure H., Hoang C. T., Radtke U., Causse C., Borel Best M., Lafont R., Bieda S., Lambeck K. (1994). Quaternary uplifted coral reef terraces on Alor island, East Indonesia: Coral reefs, 13, 215–223.

Harris, R., Vorkink, M. W., Prasetyadi, C., Zobell, E., Roosmawati, N., Apthorpe, M. (2009). Transition from subduction to arc-continent collision : Geologic and neotectonic evolution of Savu Island, Indonesia : Geosphere, 5, 152-171. doi: 10.1130/GES00209.1

Jouannic C., Hoang C. T., Hantoro W. S., Delinom R. M.,1(988); Uplift rate of coral reef terraces in the area of Kupang, West Timor: preliminary results: Palaeogeography, Palaeoclimatology, Palaeoecology, 68, 259–272. doi: 10.1016/0031-0182(88)90044-2.

Major J., Harris R., Chiang H.-W., Cox N., Shen C. C. Nelson S. T., Prasetyadi C., Rianto A. (2013). Quaternary hinterland evolution of the active Banda arc: Surface uplift and neotectonic deformation recorded by coral terraces at Kisar, Indonesia: Journal of Asian Earth Sciences, 73, 149–161. doi: 10.1016/j.jseaes.2013.04.023.

Miller, M.S., Zhang, P., Dahlquist, M.P., West, A.J., Becker, T.W., Harris, C.W. (2021). Inherited lithospheric structures control arc-continent collisional heterogeneity. Geology, 49 (6), 652–656. doi:10.1130/G48246.1.

Morley, C.K., Westaway, R. (2006). Subsidence in the super-deep Pattani and Malay basins of Southeast Asia: a coupled model incorporating lower-crustal flow in response to post-rift sediment loading. Basin Research, 18, 51-84.

Nexer, M., Authemayou, C., Schildgen, T., Hantoro, W. S., Molliex, S., Delcaillau, B., Pedoja, K., Husson, L., Regard, V. (2015). Evaluation of morphometric proxies for uplift on sequences of coral reef terraces: A case study from Sumba Island (Indonesia). Geomorphology, 241, 145-159.

Parham, P.R. (2016). Late Cenozoic relative sea-level highstand record from Peninsular Malaysia and Malaysian Borneo: Implications for vertical crustal movements: Bulletin of the Geological Society of Malaysia, 62, 91–115, doi.org/10.7186/bgsm62201612.

Pedoja, K., Husson, L., Bezos, A., Pastier, A.M., Imran, A. M., Arias-Ruiz, C., Sarr, A.C., Elliot, M., et al. (2018). On the long-lasting sequences of coral reef terraces from SE Sulawesi (Indonesia): Distribution, formation, and global significance. Quat. Sci. Rev. 188, 37-57. doi:10.1016/j.quascirev.2018.03.033.

Pirazzoli P. A., Radtke U., Hantoro W. S., Jouannic C., Hoang C. T., Causse C., Borel Best C. (1993). A one million-year-long sequence of marine terraces on sumba island, Indonesia: Marine Geology, 109, 221–236. doi:10.1016/0025-3227(93)90062-Z.

Ringor, C. L., Omura, A., and Maeda, Y. (2004). Last Interglacial Sea Level Changes Deduced from Coral Reef Terraces in Southwest Bohol, Central Philippines, Daiyonki-kenkyu, 43, 401–416, doi.org/10.4116/jaqua.43.401.

Sarr, A.C., Husson, L. Sepulchre, P., Pastier, A.-M., Pedoja, K., Elliot, M., Arias-Ruiz, C., Solihuddin, T., Aribowo, S., Susilohadi, (2019a). Subsiding Sundaland. Geology. 47, doi:10.1130/G45629.1.

Solihuddin T., Collins L. B., Blakeway D., O'Leary M. J. (2015). Holocene coral reef growth and sea level in a macrotidal, high turbidity setting: Cockatoo Island, Kimberley Bioregion, northwest Australia: Marine Geology, 359, 50-60. Doi: 10.1016/j.margeo.2014.11.011

Solihuddin T., Burafale G., Blakeway D., O'Leary M. (2016) Geomorphology and late Holocene accretion history of Adele reef: a Northwest Australian mid-shelf platform reef: Geo-Mar Letter, 36, 465-477.

Sumosusastro P., Tjia H., Fortuin A., Van Der Plicht J. (1989). Quaternary reef record of differential uplift at Luwuk, Sulawesi East arm, Indonesia: Netherlands Journal of Sea Research, 24, 277–285. doi: 10.1016/0077-7579(89)90154-3

Susilohadi, S., Soeprapto, T. A. (2015). Plio-Pleistocene Seismic Stratigraphy of the Java Sea between Bawean Island and East Java. Mar. Geol. Indones. 32, 5–16.

Wong, H. K., Lüdmann, T., Haft, C., Paulsen, A-M. (2003). Quaternary sedimentation in the Molengraaff paleo-delta, northern Sunda-shelf (Southern South China Sea): SEPM Special Publication, 76, 201-216.

Movie S1: Model simulations of the Indo-Australian subduction zone (model time in My), showing the continental topography and Indian oceanic lithosphere (blue surface and thermal structure, eastern side view).

Movie S2: Close ups of the Banda subduction zone, southward view. Indian oceanic lithosphere (blue surface) and continental units in brown (Australia) and white contours (Wallacea islands). Streamlines show mantle flow.